Properties of an electron bubble approaching the surface of liquid helium

Francesco Ancilotto and Flavio Toigo
Dipartimento di Fisica "Galileo Galilei," Università di Padova and Consorzio Interuniversitario di Struttura della Materia, Instituto Nazionale di Fisica Moleculaire, via Marzolo 8, 35100 Padova, Italy
(Received 8 April 1994; revised manuscript received 30 June 1994)

We have studied the $T = 0$ properties of the localized state of an excess electron in liquid ^{4}He using a density-functional method. The binding energy, radius, and surface tension of the electron bubble in bulk liquid ^{4}He are calculated. The modifications of the bubble properties as the electron approaches the He surface are investigated. The calculated energy barrier for thermal emission of the electron from the surface into the vacuum is found to be in agreement with the experimental value. We have calculated the escape rates for electron tunneling through the surface layer and found the results in semiquantitative agreement with the experiments.

I. INTRODUCTION

Excess electrons produced in liquid ^{4}He by a radioactive source or by cathode injection localize in a bubble-like cavity whose size is determined by a balance between the outward kinetic pressure of the electron wave packet and the inward pressure due to the surface tension and electrostriction.[1] The electron-helium repulsion is so large that a local fluid dilation leads to a stable state despite the large increase in the electron kinetic energy due to localization. Since the size of the bubble is intermediate between macroscopic and microscopic, the behavior of excess electrons in liquid helium is particularly interesting and has attracted the attention of experimentalists and theorists in the last thirty years.

The localized states of electrons in bulk liquid ^{4}He are well understood. In the simplest model the electron is confined in a spherical square well (SSW) of radius R and depth V_0. The total energy of the electron-He system can be written as[2,3] $E = E_e + 4/3\pi R^3 P + 4\pi R^2 \sigma - (\epsilon - 1)e^2/2\epsilon R$, where E_e is the ground-state electronic energy in the spherical well, the second term is the pressure-volume work done in forming the cavity, the third term is the surface energy of the bubble, and the last term is the (small) polarization energy contribution. V_0 is the lowest energy a delocalized electron can have in the liquid (conduction-band edge). Using the experimentally known quantities $\sigma = 0.378$ dyn/cm for the surface tension, $\epsilon = 1.057$ for the static dielectric constant of liquid He, and $V_0 \sim 1$ eV,[4] and minimizing E with respect to R, one gets a bubble equilibrium radius $R \sim 17$ Å at $P = 0$. A precise value for the bubble effective mass has been obtained in resonance experiments on excess electrons trapped beneath the free surface of liquid ^{4}He.[5] These measurements yielded a bubble radius $R = 17.2 \pm 0.15$ Å. Earlier theoretical calculations[6,7] yielded R between 17 and 18 Å.

Less clear is the theoretical interpretation of the experimental results where electrons produced inside the liquid are driven to the surface and then collected outside. If an electric field F is used to accelerate an electron bubble towards the free surface of the liquid, the electric force acts against the image potential $V_i(z) = Qe^2/\epsilon z$ which tends to keep the electron inside the liquid. Here z is the coordinate of the bubble normal to the surface (which is assumed to be planar and located at $z = 0$), and $Q = (\epsilon - 1)/4(\epsilon + 1) \sim 7 \times 10^{-3}$. As a result of these competing forces, the excess electron is trapped below the liquid surface in the net total potential $V_e(z) = Qe^2/\epsilon z + eFz$. V_e has a shallow minimum located several hundreds Å below the surface, depending on the value of F. When the electron, due to its thermal motion, comes sufficiently close to the surface the bubble bursts and the electron can escape into the vapor phase. It has been found[8,9] that the surface acts as a small potential barrier to the extraction of the electrons from the liquid to the vapor. The measured current due to the emitted electrons decreases rapidly with decreasing T (below the λ point) as $e^{-\Phi/k_B T}$, suggesting a thermally activated diffusion mechanism for electron escape. The barrier Φ depends on the value of the applied electric field, ranging from $\Phi/k_B \sim 30$ K to $\Phi/k_B \sim 40$ K at very low field values.[9] The theoretical interpretation of these observations has been rather crude,[8,10] attributing this barrier to the image force acting on the electron as the surface is approached from inside the liquid. The increasing polarization potential $V_i(z)$ reaches a maximum Φ and then drops abruptly when the bubble "touches" the surface layer. At this point the bubble bursts, allowing the electron to escape outside. A quantitative determination of the barrier Φ requires, however, the knowledge of the modifications of the electron potential $V_i(z)$ due to the diffuseness of the surface density profile and of the actual distance at which the bubble becomes unstable and bursts. In the absence of this important information, only semiquantitative explanations of the experimental results have been proposed so far.[8,10]

The trapping times of excess electrons in the potential well $V_e(z)$ have been measured long ago.[11] Characteristic lifetimes of the order 1–100 s have been observed, depending on the value of the temperature T and of the electric field F. Whereas the T dependence of the ob-

served lifetimes was reproduced correctly by assuming a thermal diffusion over a barrier $\Phi/k_B \sim 44$ K, the electric field dependence of the trapping time was only in fair agreement with the data. Moreover, an anomalously large curvature of the potential energy curve at the top of the barrier had to be assumed in order to fit the experimental data.[11] Thus the possibility of electron tunneling has been proposed[12] as an alternative mechanism for the observed electron emission, where the electron moves by thermal motion towards the surface and then decays by quantum tunneling into the vapor phase. The barrier height experienced by the electron near the surface is roughly $V_0 - E_e$, where V_0 is the conduction-band edge and E_e is the zero-point energy of the electron in the bubble cavity. Within the tunneling model,[12] the observed trapping times can be related to the bubble parameters (radius R and binding energy $E_b \equiv V_0 - E_e$), which could thus be derived from a fit to the experimental data. The resulting $R \sim 25$ Å is, however, too large compared to the experimental value $R \sim 17$ Å. A more refined calculation was performed later,[13] where the electron tunneling rates were computed using the transfer Hamiltonian method of Bardeen,[14] rather than a semiclassical WKB method as done in Ref. 12, but still a bubble radius $\sim 50\%$ larger than the experimental value had to be assumed in order to give results in agreement with experiments. If the physical bubble radius ($R \sim 17$–18 Å) is used instead, lifetimes a few hundred times larger than the experimental values are obtained.

We present here the results of calculations, performed within a density-functional approach, where the behavior of the electron bubble as it approaches the free surface of liquid ^{4}He is investigated. A value $R = 17.9$ Å is found for the bubble radius in the bulk liquid, in agreement with previous theoretical and experimental determinations. We find that up to an electron-surface distance of $d_0 \sim 23$ Å the bubble is stable, while at lower distances it becomes unstable and bursts, allowing the electron to escape into the vapor. A potential energy barrier $\Phi/k_B \sim 38$ K for the thermal emission of electrons is obtained from our results, whose value compares favorably with the experimental results quoted above.

The electron, however, can still escape into the vapor by quantum tunneling even when the electron-surface distance d is larger than d_0, i.e., from the region where the bubble is "mechanically" stable. We have calculated the decay times τ of the electron current from a direct solution of the bubble diffusion equation including a loss term to allow for electron tunneling.

Two major ingredients enter the definition of the decay rate $P \equiv \tau^{-1}$, i.e., the tunneling matrix elements $p(z)$, which depend exponentially on the electron-surface distance z, and the bubble distribution function $n(z)$, which determines the probability of a bubble being at a distance z from the surface. We find that the interface structure and diffuseness have a very small effect on $p(z)$, whose calculated values are very close to those obtained in a simplified model where both the bubble-liquid and liquid-vacuum interfaces are sharp. We find, however, at variance with previous theoretical calculations where a Boltzmann-like distribution function n_{eq} was assumed,[12,13] that $n(z)$ deviates largely from the equilibrium form n_{eq} in the region close to the surface layer where tunneling is most effective in destroying bubbles. As a consequence, our calculated lifetimes τ are much smaller than those obtained under the hypothesis $n \sim n_{eq}$[12,13] and in semi-quantitative agreement with the experimental values.

In Section II we describe the method, based on a density-functional approach, that we use to calculate the static properties of the electron bubble and its energy as a function of the distance from the surface. In Sec. III we present our results for the electron in bulk liquid He while in Sec. IV the effects of the liquid He surface on the bubble properties are investigated. Section V contains the results of calculations, based on the results of Sec. IV, where the tunneling decay rates of the liquid-to-vacuum electron current are computed from a direct solution of the bubble diffusion equation. A few concluding remarks are provided in Sec. VI.

II. COMPUTATIONAL METHOD

A phenomenological density-functional (DF) approach to study the properties of the ^{4}He liquid-vapor interface has been proposed recently,[15] which gives a good description of the $T = 0$ bulk liquid equation of state and of the properties of the free surface, once the few parameters entering the functional definition are fixed to reproduce some experimental values. The surface density profile of the liquid has been obtained from the functional of Ref. 15 and found to be in good agreement with x-ray diffraction measurements[16] and with *ab initio* Monte Carlo cluster calculations.[17]

This functional, which is based on a zero-range Skyrme-type interaction, has been recently extended to include the effect of the finite-range He-He interaction.[18] The resulting DF reproduces also the behavior of the static density-density response function of the bulk liquid, the static polarizability and the actual surface energy at $T = 0$. This energy functional has the form[18]

$$E_l[\rho] = \frac{\hbar^2}{2M}\int [\nabla \rho^{1/2}(\vec{r})]^2 d\vec{r} + \frac{1}{2}\int\int d\vec{r}\,d\vec{r}\,'\rho(\vec{r})\rho(\vec{r}\,')V_l(|\vec{r}-\vec{r}\,'|) + \frac{c}{2}\int \rho(\vec{r})(\bar{\rho}_r)^{1+\gamma} d\vec{r}, \quad (1)$$

where ρ is the liquid density and M is the ^{4}He atomic mass. The first term is the quantum kinetic energy term, the second term contains a two-body He-He pair potential $V_l(r)$ screened at distances shorter than a characteristic length h, while the last term, which contains the average $\bar{\rho}_r$ of the density over a sphere of radius h and which is always positive, accounts for the internal kinetic energy and for the increasing contribution of the hard-core He-He repulsion when the density is increased. The three free parameters h, c, γ are adjusted in order to reproduce the experimental values of the energy per atom

for liquid ^{4}He, the compressibility of bulk liquid at the saturation density, and the surface tension σ. The surface structure of the liquid has been obtained in Ref. 18 by minimizing the energy functional in Eq. (1) with respect to ρ, with the constraint of fixed number of He atoms, $\int \rho(\vec{r})d\vec{r} = N$, and by imposing the boundary condition $\rho(\vec{r}) = \rho_0$ far from the surface.

We have used the above functional to study the behavior of an excess electron in liquid He. If $w(r)$ represents the electron-helium two-body interaction potential, then the functional

$$E_e[\rho,\Psi] = \frac{\hbar^2}{2m}\int |\nabla\Psi(\vec{r})|^2 d\vec{r} + \int\int \rho(\vec{r})|\Psi(\vec{r}')|^2 w(|\vec{r}-\vec{r}'|)d\vec{r}d\vec{r}' \quad (2)$$

gives the energy of the electron in the liquid.

If the electron wave function $\Psi(\vec{r})$ varies slowly over distances of the order of the mean interatomic separation, $\rho^{-1/3}$, the condition of minimum of the total energy $E = E_l + E_e$ with respect to ρ and Ψ, subject to the constraints $\int \rho(\vec{r})d\vec{r} = N$ and $\int |\Psi(\vec{r})|^2 d\vec{r} = 1$, yields the two equations

$$\left[-\frac{\hbar^2}{2m}\nabla^2 + \int w(|\vec{r}-\vec{r}'|)\rho(\vec{r}')d\vec{r}'\right]\Psi(\vec{r}) = \epsilon_e\Psi(\vec{r}) , \quad (3a)$$

$$\left[-\frac{\hbar^2}{2M}\nabla^2 + V_{\rm eff}(\vec{r})\right]\Phi(\vec{r}) = \epsilon_{\rm He}\Phi(\vec{r}). \quad (3b)$$

In the second equation $\Phi(\vec{r}) \equiv \rho^{1/2}(\vec{r})$ is the helium total wave function. The above equations self-consistently determine the extremal wave function Ψ and the density profile ρ. Equation (3b) follows from the usual condition of local equilibrium for a fluid in the slowly varying "external" potential $\int w(|\vec{r}-\vec{r}'|)|\Psi(\vec{r}')|^2 d\vec{r}'$.[19] The helium effective potential $V_{\rm eff} \equiv \delta E/\delta\Phi(\vec{r})$ is given explicitly by

$$V_{\rm eff}(\vec{r}) = \int \rho(\vec{r}')V_l(|\vec{r}-\vec{r}'|)d\vec{r}' + \frac{c}{2}(\bar{\rho}_r)^{\gamma+1} + \frac{c}{2}(1+\gamma)\int d\vec{r}'\rho(\vec{r}')(\bar{\rho}_{r'})^{\gamma}\Pi_h(|\vec{r}-\vec{r}'|) + \int d\vec{r}' w(|\vec{r}-\vec{r}'|)|\Psi(\vec{r}')|^2, \quad (4)$$

where $\Pi_h(r) = 3/(4\pi h^3)$ when $r < h$ and $\Pi_h = 0$ otherwise.

Our calculations have been performed using a periodically repeated supercell containing one electron and N helium atoms. To model the electron-helium interaction $w(r)$ we used the pseudopotential described in Ref. 20, which has been used in several theoretical calculations and which reproduces the experimental data for low-energy electron-helium elastic scattering. We expand the electron and He wave functions Ψ,Φ and the associated densities $\rho_e \equiv |\Psi|^2$ and ρ in plane waves: $\Psi(\vec{r}) = \sum_{\vec{G}} C^{(e)}_{\vec{G}} e^{i\vec{G}\cdot\vec{r}}$, $\Phi(\vec{r}) = \sum_{\vec{G}} C_{\vec{G}} e^{i\vec{G}\cdot\vec{r}}$, and similarly for ρ and ρ_e. The $\vec{G}$'s are the supercell wave vectors, $\vec{G} = \pi(n/L_x, m/L_y, p/L_z)$, with $n,m,p = 0,\pm1,\pm2,...$ and L_x, L_y, L_z are the sides of the supercell. A kinetic energy cutoff is used to make the computations feasible, such that the maximum wave vector $G_{\rm max}$ in the Fourier expansions satisfies $G^2_{\rm max}/2 < E_{\rm cut}$. We choose $E_{\rm cut} = 1.5$ Ry. We checked that by further increasing this cutoff, the total energy and the structural parameters of the electron bubble do not change significantly.

Consider the gradients of the total energy $\partial E/\partial C_{\vec{G}}$ and $\partial E/\partial C^{(e)}_{\vec{G}}$, where

$$\partial E/\partial C_{\vec{G}} \equiv (1/\Omega)\int (\delta E/\delta\Phi)\exp(-i\vec{G}\cdot\vec{r})\, d\vec{r}, \quad (5)$$

and similarly for $\partial E/\partial C^{(e)}_{\vec{G}}$ (Ω is the volume of the supercell). A variety of algorithms exist that allow one to use the gradients in order to reach the minimum of energy functionals, and which can be competitive with the usual self-consistent matrix diagonalization of the one-particle Hamiltonians.[21]

Let $\{C_{\vec{G}}\}$ and $\{C^{(e)}_{\vec{G}}\}$ denote the two sets of coefficients of the Fourier decomposition of a given initial Ψ and Φ. The simplest choice is to move iteratively the $\{C_{\vec{G}}\}$ and $\{C^{(e)}_{\vec{G}}\}$ in the direction opposite to the gradients, following a steepest descent (SD) path, where $\partial E/\partial C_{\vec{G}}$ and $\partial E/\partial C^{(e)}_{\vec{G}}$ play the role of forces driving the system to the minimum energy configuration. This approach is equivalent to solving the first-order equations of motion (the dot means time derivative)

$$\mu\dot{C}_{\vec{G}} = -\partial E/\partial C_{\vec{G}}, \qquad \mu_e\dot{C}^{(e)}_{\vec{G}} = -\partial E/\partial C^{(e)}_{\vec{G}}, \quad (6)$$

with the additional constraints $\int \rho(\vec{r})d\vec{r} = N$ and $\int |\Psi(\vec{r})|^2 d\vec{r} = 1$. Here μ and μ_e are arbitrary parameters ("masses"), which control the inertia of the coefficients C_G,$C^{(e)}_G$ during their time evolution. The above equations can be solved in practice by time discretization: $C_{\vec{G}}(t+\Delta t) \sim C_{\vec{G}}(t) + (\Delta t/\mu)(-\partial E/\partial C_{\vec{G}})$, with an appropriate choice of the time step Δt. The simple algorithm embodied in Eq. (6), although very easy to implement, is usually not very efficient, since it requires a number of steps of the order of thousands to converge to the minimum of the total energy E. We improved the efficiency of this algorithm by alternating SD moves with a second-order dynamics scheme, where the Fourier expansion coefficients of Ψ and Φ are updated according to a fictitious Newton dynamics:

$$\mu\ddot{C}_{\vec{G}} = -\partial E/\partial C_{\vec{G}}, \qquad \mu_e\ddot{C}^{(e)}_{\vec{G}} = -\partial E/\partial C^{(e)}_{\vec{G}} , \quad (7)$$

subject to the same constraints on the electron wavefunction normalization and on the conservation of the number of He atoms. The above constrained equations have the same form as those used in the usual molecular dynamics (MD) algorithm. We define a "work" per unit time $W = {\rm Re}\{\dot{C}_G(-\partial E/\partial C_G)\}$, $W^{(e)} =$

$\mathrm{Re}\{\dot{C}_G^{(e)}(-\partial E/\partial C_G^{(e)})\}$. If W ($W^{(e)}$) is ≥ 0, we update the wave function Φ (Ψ) according to the second-order MD equations Eq. (7), otherwise we make a SD move with Eq. (6). The MD moves, when permitted, allow the electron-He system to roll down the energy surface increasing the kinetic energy of the previous time step, as in conventional MD calculations. If, on the other hand, the powers W,$W^{(e)}$ are negative, then a downhill movement with zero initial velocities is performed according to a SD algorithm. The second-order equations Eq. (7) are integrated in practice using a simple Verlet algorithm at discrete time steps.

The mixed MD-SD scheme outlined above, which has been used previously in *ab initio* total energy calculations,[22] is found to greatly reduce the computer time required to attain the minimum of the total energy, compared with a pure SD algorithm. In Fig. 1 we show an example of the reduction that can be achieved with this scheme. We plot here the logarithm of the deviation of the total energy E from the ground-state energy E_0 of the electron-He system vs the number of integration steps during a minimization cycle. It appears that a much faster convergence rate can be achieved with the MD-SD scheme compared to SD, at least in the first stage of the minimization procedure. Eventually, the MD-SD dynamics results in a slower convergence rate than pure SD. After a number of steps of the order of 100–200 with the MD-SD algorithm, it is thus convenient to switch to SD to converge with optimum efficiency towards the minimum. In spite of its simplicity, the MD-SD scheme improves substantially the rate of convergence of the wave functions to the ground state and makes it comparable with that provided by other, more sophisticated, schemes used in total energy DF calculations, such as the conjugate-gradient method described in Ref. 23.

A step of minimization with the above scheme requires the calculations of the various terms in the gradients $\partial E/\partial C_{\vec{G}}$ and $\partial E/\partial C_{\vec{G}}^{(e)}$ and in the total energy $E = E_l + E_e$. Each term is calculated in the most convenient space (real or Fourier). The transformations between real and reciprocal space are done efficiently by using standard fast Fourier routines.

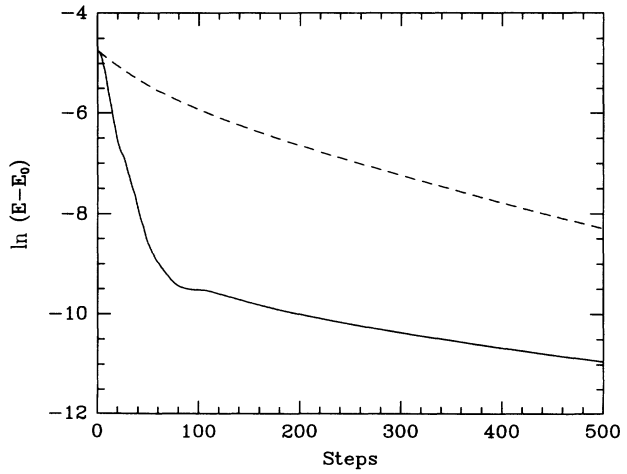

FIG. 1. Natural logarithm of the deviation of the total energy E from the ground-state energy E_0 (in atomic units) vs the number of integration steps. Dashed line: steepest descent algorithm. solid line: molecular dynamics–steepest descent algorithm.

III. THE ELECTRON BUBBLE IN BULK LIQUID ^{4}HE

We have studied the bulk liquid case first, where an excess electron is present in liquid ^{4}He, at the saturation density $\rho_0 = 2.184 \times 10^{-2}$ Å^{-3}. We used a periodically repeated cubic cell of side 68 Å. In the initial configuration the He fills the cell except at the center of it, where a sharp spherical hole is cut, containing a Gaussian electron wave function of width much smaller than the hole diameter. The system is then allowed to relax to the configuration of minimum total energy via MD-SD dynamics. Due to the periodic boundary conditions, some care must be used to chose the correct number of He atoms in the supercell, in such a way that the final state where the bubble is fully relaxed shows the correct asymptotic value of the density $\rho(r) = \rho_0$ close to the cell boundaries.

We show in Fig. 2 the final electron and helium density profiles in a plane passing through the center of the cell (where the maximum of the electron charge density is located). The He density shows a rather steep profile at the bubble interface, with a t_{10-90} width of the interface layer of 4.4 Å, i.e., smaller than the value $t_{10-90} = 5.9$ Å for the ^{4}He free surface.[18] If we *define* the bubble radius as the radius of the spherical surface where $\rho(r) = \rho_0/2$, we find $R = 17.9$ Å, in agreement with the experimental value $R = 17.2$ Å.[5]

In Fig. 3 we show the self-consistent electron potential $\int w(|\vec{r} - \vec{r'}|)\rho(\vec{r'})d\vec{r'}$. It appears that far from the electron center the potential approaches a constant value $V_0 = 1.48$ eV. This value represents the potential energy of a delocalized electron in a homogeneous liquid of density ρ_0, $V_0 = \rho_0 \int w(r)d\vec{r}$, i.e., is the definition of the conduction-band edge in our continuum model for the

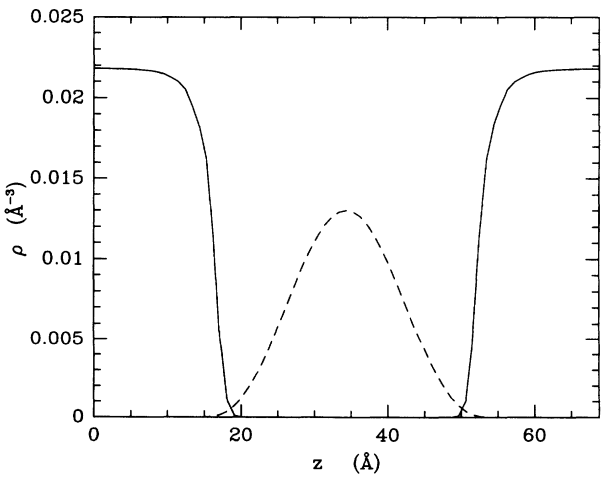

FIG. 2. Density profiles for an electron bubble in bulk liquid He. Solid line: helium density. Dashed line: electron charge density.

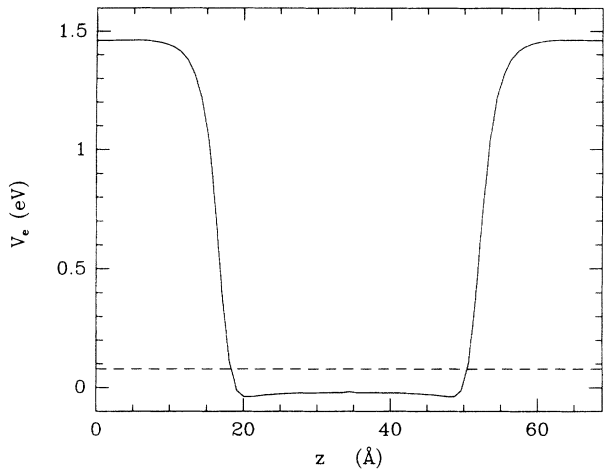

FIG. 3. Electron self-consistent potential profile in a plane passing through the maximum of the electron charge density. The dashed line shows the electron energy level E_e.

liquid. Experimental determinations of V_0 at the saturation density ρ_0 range from 0.95 eV (Ref. 24) to 1.3 ± 0.4 eV.[25] If we take as representative of V_0 the accurate result of Ref. 26, $V_0 = 1.1 \pm 0.1$ eV, we see that our calculated conduction band edge is $\sim 30\%$ larger than the experimental value. The reason for this discrepancy is the following. Our definition for V_0 is just the energy of a quasi-free-electron state with wave vector $k = 0$ in the unperturbed homogeneous fluid of density ρ_0 as given by first-order perturbation theory. At low electron-He distances the repulsive part of the interaction potential w is too large for the perturbation theory to be applicable and this leads to an overestimate of the interaction energy. A more accurate calculation of V_0, including many-body polarization effects[27] and using the same pseudopotential used here to model the electron-He interaction, gives values of the conduction-band edge in good agreement with experiments.

Our overestimate of V_0 is thus not related to a poor representation of the electron-helium interaction potential, but is rather an inescapable consequence of our continuum model description of the host liquid. This overestimate is expected to have little consequence on the static properties of the electron bubble described in this section and in Sec. IV, since a change in V_0 results in tiny variations of the exponential tail of the electron wave function in the liquid side. For instance, within the SSW model mentioned in the Introduction, a decrease of V_0 from our calculated value $V_0 = 1.48$ eV to the experimental value $V_0 \sim 1$ eV results in a 1.7% decrease of the bubble radius, while the electron bubble energy E_e decreases by 2.5%.

However, variations in V_0 are expected to have a large effect on the electron tunneling matrix elements calculated in Sec. V, where small changes in the potential barrier height $(V_0 - E_e)$ can alter substantially the calculated escape rates, due to the exponential dependence of these rates on $(V_0 - E_e)$. For this reason in the evaluation of the tunneling probabilities we must correct our results in order to incorporate the experimental value of V_0, as will be discussed in Sec. V.

Our calculated electron energy $E_e = E_{\text{kin}} + E_{e\text{-He}} = 0.092 - 0.013 = 0.079$ eV, shown with a dashed line in Fig. 3, is smaller than the ground-state $E_e = 0.12$ eV calculated with the simple spherical square well model which is often used to describe the bubble state in bulk liquid,[3] and comparable with the result $E_e = 0.07$ eV obtained in the variational calculations reported in Ref. 6. A value for the bubble binding energy $E_b = V_0 - E_e = 1.02$ eV is obtained if we use the experimental value $V_0 = 1.1$ eV.[26]

We have calculated the bubble surface energy $\sigma_b \sim (E_l - N\epsilon_0)/4\pi R_b^2$, where E_l is the helium total energy, $\epsilon_0/k_B = 7.18$ K is the energy per ^{4}He atom in the uniform bulk liquid, and N is the total number of He atoms in the supercell (in the present case $N = 6500$). R_b is the radius of the Gibbs dividing surface[28] $R_b = \{\rho_0^{-1} \int r^3 [d\rho(r)/dr] dr\}^{1/3} = 18.7$ Å. We find $\sigma_b = 0.360$ dyn/cm, i.e., $\sim 5\%$ smaller than the value we find for the free surface, $\sigma = 0.381$ dyn/cm, showing that the curvature contribution to the surface tension is rather small and negative in sign. This result agrees with the phenomenological DF calculations of Ref. 28.

We have also calculated the bubble parameters R, σ, and E_b in bulk liquid at a higher density $\rho = 0.0231$ Å^{-3}, i.e., the experimental He density at a pressure $P = 5$ atm and $T = 2.2$ K. We find $\sigma = 0.544$ dyn/cm, $R = 14.5$ Å, and $E_b = 1.03$ eV, respectively. The binding energy $E_b = V_0' - E_e$ does not change appreciably at the higher density because the increase in the electron ground-state energy E_e due to the smaller bubble radius is balanced by the increase in the conduction-band edge V_0' (which scales roughly linearly with the liquid density).

IV. THE ELECTRON BUBBLE APPROACHING THE SURFACE OF LIQUID ^{4}He

Having obtained reliable results for the electron bubble parameters in bulk liquid, we include in our calculations the presence of a free surface. Our repeated supercell now contains a thin slab of liquid He delimited by two planar surfaces. The cell length is 64 Å along the x, y directions and 120 Å along the z direction. The surfaces delimiting the He slab are parallel to the x-y plane. The slab thickness is ~ 94 Å and a vacuum region ~ 26 Å wide is used to decouple the slab from its repeated images along the z direction. The thickness of the slab is found sufficient to decouple the two surfaces delimiting the film, i.e., in the absence of the extra electron the correct density profile for the two free surfaces is obtained. The lateral size of the cell is the minimum one that gives converged results for the bubble radius and formation energy, when the excess electron is present.

In our initial configuration a sharp spherical cavity is cut at the center of the slab, where a Gaussian electron wave function is placed. We then proceed with the simultaneous minimization of the total energy E with respect to Ψ and Φ. We made a number of calculations where the electron is placed at different distances from the upper surface of the He film. We find that up to rather small electron-surface distances the final state is

stable, i.e., the bubble does not burst. The minimum energy electron and He densities for three different electron positions are shown in Fig. 4 by means of contour lines. The electron-surface distances in the three cases shown in Fig. 4 are $d = 46$, 26, and 23 Å, respectively: d is defined as the distance separating the maximum of the electron density from the surface plane where $\rho(r) = \rho_0/2$. At the distance of closest approach [panel (c)] the thickness of the surface layer separating the electron from the vacuum side is only ~ 6 Å, i.e., of the order of two atomic layers. It also appears from panel (c) in Fig. 4 that the thin liquid layer separating the electron from the vacuum side has a somewhat lower density than the bulk value ρ_0.

In Fig. 5 we show the electron self-consistent potential profiles for the same configurations as in Fig. 4. Only the part of the slab close to the upper surface is shown. The decrease in the liquid density in front of the bubble as the electron approaches the surface results in the lowering of the potential barrier which keeps the electron inside the liquid. This lowering, as will be shown in the next section, affects to some extent the calculated escape rates when the electron is allowed to flow outside the bubble cavity by quantum tunneling.

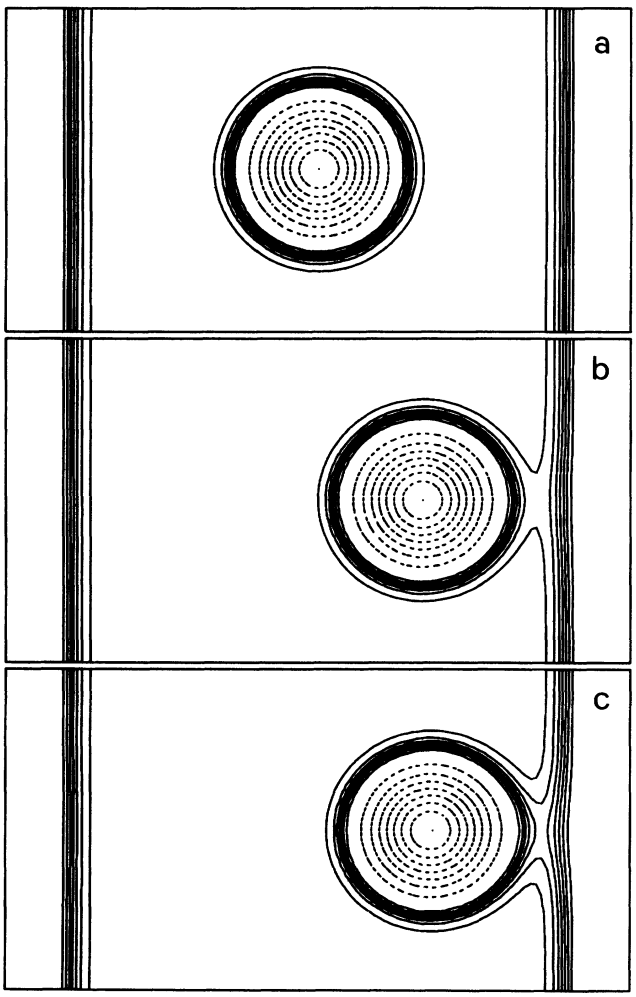

FIG. 4. Contour plots of the electron and helium densities for three different positions of the electron bubble. The solid lines show the He density, the dotted lines the electron density $|\Psi|^2$. The plane where the contours are drawn cuts the slab parallel to the x-y surface plane and passes through the maximum of the electron charge density. (a) Electron-surface distance $d = 46$ Å. Panel (b) $d = 26$ Å. Panel (c) $d = 23$ Å.

The dotted lines in Fig. 5 show the electron energy $E_e = E_{\text{kin}} + E_{e\text{-He}}$. Although on the scale of Fig. 5 the electron energy seems to be fairly constant for the three configurations shown, there are, however, minute variations of E_e as the electron-surface distance varies. These small changes are important because they determine the potential energy barrier for thermal emission of the electron from the liquid into the vacuum side. Before evaluating this quantity, however, we must correct our calculated values for E_e to take into account the long-range tail of the electron-helium polarization potential which is truncated at the lower surface of the He slab in our calculations. If we treat the electron as a point charge, we must add to E_e a term $-Qe^2/\tilde{d}$, where $\tilde{d}$ is the distance of the electron center from the lower surface of the slab, and again $Q = (\epsilon - 1)/4(\epsilon + 1)$.

The variations in the calculated electron energy $E_e = E_{\text{kin}} + E_{e\text{-He}}$, with the long-range correction included, are shown as a function of the electron-surface distance in Fig. 6(a) (squares). The zero of the energy scale in Fig. 6(a) is taken at the value of the electron energy in an infinitely extended bulk liquid, $E_e' \sim E_e^c - 2Qe^2/L_{1/2}$, where E_e^c is the calculated energy of an electron in the middle of the slab [see panel (a) in Fig. 4], and $L_{1/2} = L_z/2$ is the slab half-thickness.

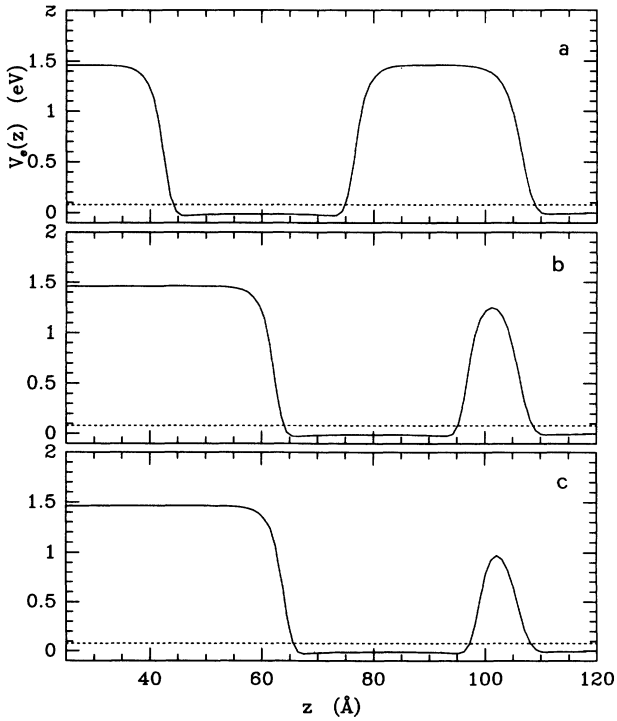

FIG. 5. Electron potential profile for the three configurations shown in Fig. 4. The dotted lines show the electron energy level E_e.

The variation in the helium total energy $E_l - E_l^c$ with the bubble-surface distance is shown in Fig. 6(b). The zero of the energy scale is taken at the value of E_l when the bubble is in the middle of the slab, well below the surface ("bulk" value E_l^c). The energy difference shown in Fig. 6(b) is approximately constant when the bubble is far from the surface, whereas it becomes lower by ~ 15 K than its bulk value as the bubble approaches the surface. This energy gain with respect to the bulk value can be understood by recalling that the surface tension depends strongly on the density, $\sigma \propto \rho^4$. In the configurations where the electron is close to the surface the decrease in the He density at the surface layer results in a decrease of the bubble surface energy.

The dots in panel (a) of Fig. 6 show the overall (electron+helium) bubble energy variation. From this curve one can immediately extract a value for the potential barrier Φ_0 that an electron has to overcome to be thermally emitted from the surface, $\Phi_0 \sim 38$ K, which is in good agreement with the value $\Phi_0 \sim 40$ K (extrapolated to zero electric field) provided by experiments.[9]

For electron-surface distances lower than $d_0 \sim 23$ Å the localized bubble state appears to be unstable and the electron-He system invariably evolves during the total energy minimization towards a state of minimum energy where the electron is *outside* the surface (and completely delocalized in the x-y plane) while the empty bubble cavity has disappeared, restoring a flat liquid surface.

Some configurations of the electron-helium system during a steepest descent minimization are shown in Fig. 7. In the initial configuration the electron is at $d =$ 22 Å from the surface, i.e., just below the edge of stability d_0. The time step used is $\Delta t = 0.02$ ps and the pictures are taken every 500 time steps. The total duration of the process shown in Fig. 7 is thus 60 ps. Initially, a spherical bubble state develops, similar to the stable configuration shown in panel (c) of Fig. 4. As the minimization proceeds, the density of the surface layer separating the electron from the vacuum starts to decrease and the electron begins to spill outside by quantum tunneling, until the potential energy barrier confining the electron in the bubble cavity becomes comparable with the electron energy E_e. At this point the bubble bursts and the electron flows outside, becoming completely delocalized in the x-y plane parallel to the surface. The hole in the liquid widens and the cavity distorts. In the final configuration (not shown) the liquid restores a flat, homogeneous surface and the cavity has disappeared.

We remark that the SD fictitious dynamics which determines the sequence in Fig. 7 has little to do with the true time evolution of the e-He system,[29] the only relevant configuration being the final one, where minimum energy is achieved. In particular, the time scale of the process shown is completely arbitrary, being determined by the fictitious masses μ and μ_e used in the first-order equations (6). However, during the SD simultaneous optimization of the electron and He wave functions, we observe that the "fake" kinetic energy associated with the fictitious dynamics of the electron, $E_f = \mu_e \int |\dot{\Psi}|^2 d\vec{r}$, remains at each time step always $\sim 10^{-4}$–10^{-5} times smaller than the electron energy E_e, i.e., the electron states shown in the figure are very close to the Born-Oppenheimer surface relative to the instantaneous he-

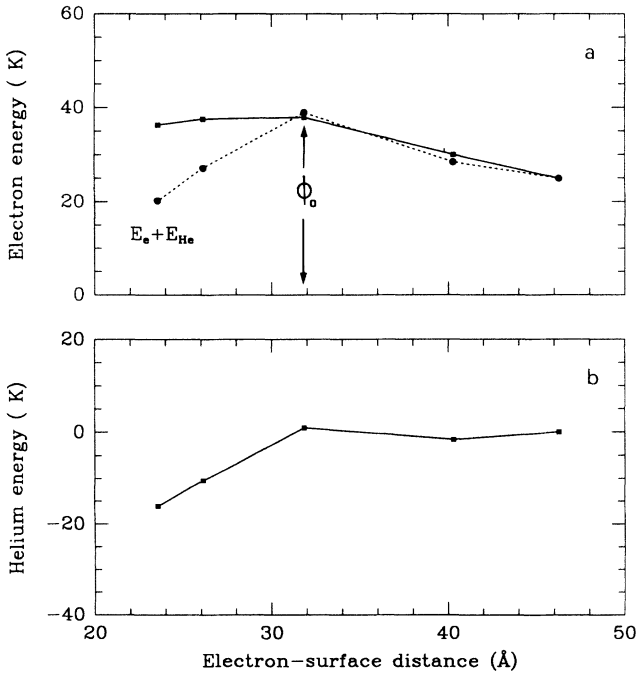

FIG. 6. Electron and helium total energy variations as a function of the electron-surface distance. The lines are only a guide to the eyes. (a) The squares show the electron energy variations. Dots: sum of the electron + helium energy variations. (b) Helium total energy variation.

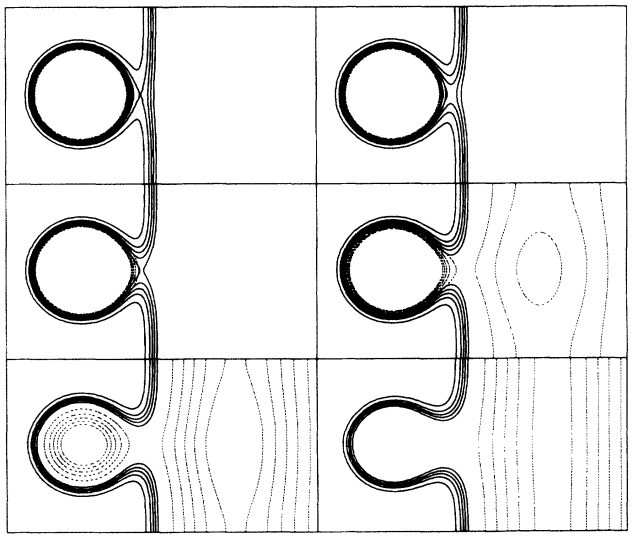

FIG. 7. Contour plots showing a sequence of electron-helium configurations during a SD minimization. From left to right and from top to bottom, in order of increasing time. The pictures are taken every 500 time steps. The solid lines show the helium density, the dotted line the electron charge density. For clarity, only the electron charge density values lower than $0.03\rho_{\max}$ are shown, $\rho_{\max}$ being the electron charge density at the center of the bubble cavity.

lium configuration. The sequence of Fig. 7 should thus represent a physical path in the electron-He phase space, although not necessarily that followed during the actual escape process.

Two different time scales are expected to control the escape of electrons from the surface of liquid He. The first is the "transit time" τ_e of the electron from the bubble to the vacuum side and the second is the time τ_l required for the density readjustments when the liquid tries to restore a flat surface. If we assume that the main mechanism of electron emission is tunneling, then the electron transit time can be estimated by means of the "traversal time"[30] $\tau_e \sim ma/\hbar\kappa$, $\kappa = \sqrt{2m(V_0 - E_e)}/\hbar$ being the imaginary momentum under the barrier. If we take $a \sim 6$ Å for the width of the He barrier (see Fig. 5), then $\tau_e \sim 10^{-15}$ s. The time τ_l is of the order of $\sim 2R/v_s \sim 10^{-11}$ s, where $v_s \sim 240$ m/sec is the sound velocity in ^{4}He and R is the bubble radius. Even such a rough argument suggests a picture where (just as in Fig. 7) the electron tunnels out rapidly leaving an empty bubble behind, while the He relaxes with a much longer time scale.

V. ESCAPE RATES OF ELECTRONS FROM THE SURFACE OF LIQUID ^{4}HE

As discussed in Sec. I, an alternative explanation to thermal diffusion over the image potential barrier has been proposed to interpret the experimental results for electron emission from the surface of liquid He, which is based on the possibility of quantum tunneling from the bubble to vacuum.[12,13] In Refs. 12 and 13 the rate P which governs the decay of the electron current from the surface to the vapor was calculated as

$$P = \frac{\int_0^\infty p(z) n_{\rm eq}(z) dz}{\int_0^\infty n_{\rm eq}(z) dz}, \tag{8}$$

where $p(z)$ is the electron tunneling probability per unit time from bubbles at a distance z from the surface and $n_{\rm eq}(z) = Ae^{-\beta V(z)}$ is the assumed bubble distribution when the electron source in the liquid is turned off, $V(z)$ being the total potential energy of the bubble electron (i.e., tunneling is neglected in the determination of $n_{\rm eq}$).

Since the resulting characteristic decay times $\tau \equiv P^{-1}$ computed using the physical bubble radius $R \sim 17$–18 Å are 200–300 larger than the experimental ones[12,13] and can be reconciled with the experimental data only by assuming a bubble radius $\sim 50\%$ larger than that found experimentally, we have reexamined both ingredients entering Eq. (8), i.e., the tunneling probability per unit time $p(z)$ and the bubble distribution.

A. Tunneling probabilities

To evaluate the tunneling rates $p(z)$ we used the transfer Hamiltonian theory of Ref. 14. In this theory, the probability per unit time for the transition $|\Psi_{\rm in}\rangle \to |\Psi_{\rm out}\rangle$ is given by $p(z) = (2\pi/\hbar)|M|^2\rho_f$, where $M = -\hbar^2/2m[\Psi^*_{\rm out} d\Psi_{in}/dz - \Psi^*_{\rm in} d\Psi_{\rm out}/dz]|_{z_b}$ is the tunneling matrix element and $\rho_f = mL/2\pi\hbar^2 k$ is the one-dimensional density of final states with wave vector $k = (2mE_e)^{1/2}/\hbar$ (we assume that the electron wave functions are normalized in a box of length L). z_b is an arbitrary point located in the barrier region.[31] $\Psi_{\rm in}$ represents the electron wave function of a stable bubble state with energy E_e, while $\Psi_{\rm out}$ refers to a state in the continuum, with the same energy E_e, where the electron is outside the He surface.

An electron above (outside) the liquid surface of helium is subject to the image potential $-Qe^2/z$.[1] Here $z = 0$ is the position of the liquid-vacuum interface, which is assumed to be planar and infinitely sharp. In the simplest model, the surface is treated as a barrier of infinite height, forcing the electron wave function to be zero at the liquid-vacuum interface.[1] In a more realistic model, at short distances the electron experiences a repulsive barrier of height $\sim V_0$, the conduction-band minimum, which inhibits penetration into the liquid. Moreover, the surface density profile is not infinitely sharp. In order to take into account the diffuseness of the liquid-vacuum interface, one must solve the one-dimensional problem where both the electron wave function and the liquid density profile ρ are allowed to adjust self-consistently. However, due to the weak binding of an external electron, we can make the reasonable assumption that the density profile of the He surface in the presence of the external electron is essentially that of the free surface. To determine $\Psi_{\rm out}$ we thus solve numerically the one-dimensional Schrodinger equation for an electron of energy E_e in the external potential $V_{\rm out} = \int \rho_f(\vec{r}) w(|\vec{r} - \vec{r}'|)$, $\rho_f(\vec{r})$ being the density profile of the *free* He surface. The calculated potential profile $V_{\rm out}$ is shown in Fig. 8 with a solid line, together with its limiting expression for large distances (dashed line), where it tends to the polarization limit $V_{\rm out} \to -Qe^2/z$.[32]

From the knowledge of $\Psi_{\rm in}$ and $\Psi_{\rm out}$ we can calculate the tunneling times $\tau_t(z) = p(z)^{-1}$ by using Bardeen's formula. Our results are shown in Fig. 9 (with dots) as a function of the electron-surface distance. For com-

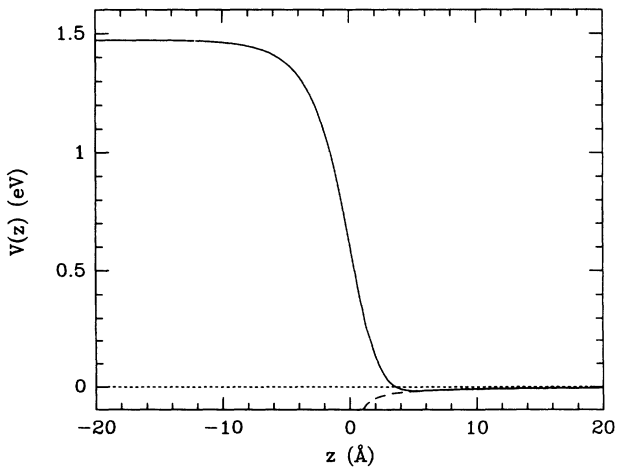

FIG. 8. Potential energy curve for an electron outside the helium surface. The dashed line shows the ideal image potential $V_i = -Qe^2/z$.

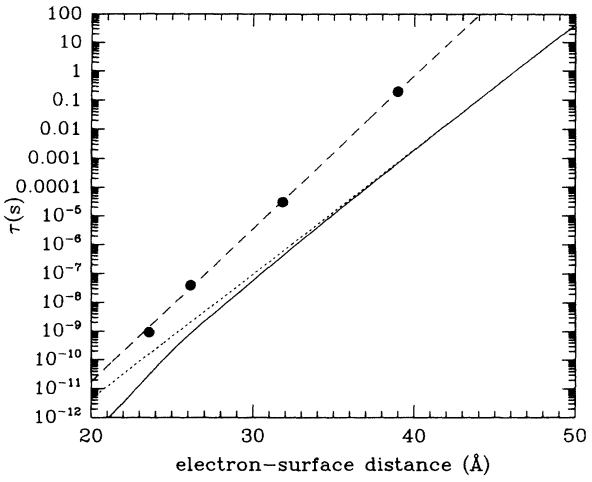

FIG. 9. Calculated electron tunneling times $p(z)^{-1}$ as a function of the electron-surface distance z. Dots: our calculated values, with $V_0 = 1.48$ eV. Dashed line: calculated as in Ref. 13, with $R = 17.9$ Å and $V_0 = 1.48$ eV. Dotted line: same as in Ref. 13, with $R = 17.9$ Å and $V_0 = 1$ eV. Solid line: same as in Ref. 13, with $R = 17.9$ Å, $V_0 = 1$ eV, and taking into account the reduction of the potential barrier height as the electron approaches the surface.

parison, we show with a dashed line the tunneling times calculated as in Ref. 13, i.e., with Bardeen's theory but using the SSW model for the bubble and a sharp liquid-vacuum boundary. Apart from slight differences at the smaller distances, the two calculations give almost coincident results, showing that the tunneling times are not affected in a significant way by the diffuseness of the bubble surface and of the liquid-vacuum interface. We may then assume that the analytic results obtained in Ref. 13 are a very good approximation also in the case of diffuse interfaces.

For the purpose of comparison with the experimental results, we must correct our results for $p(z)$ to take into account our overestimate of the conduction-band edge value V_0 (see Sec. III). To this end, we insert the experimental value $V_0 \sim 1$ eV in Eq. (25) of Ref. 13 to get the curve shown with a dotted line in Fig. 9. Moreover, if we also take into account the reduction in the potential barrier height V_0 with the electron-surface distance (see Fig. 5 and the related discussion), we obtain the results reported with the solid line in Fig. 9. Since the calculated values of $p(z)$ are basically the same as those calculated by Cole and Klein,[13] the discrepancy between theory and experiment for the electron current decay time must be due to the other ingredient entering the evaluation of P, i.e., the bubble distribution function.

B. Electron bubble distribution function

As mentioned above, in Refs. 12 and 13 it was assumed that the bubble distribution entering the determination of the current decay rate P was the equilibrium distribution $n_{eq}(z) = Ae^{-\beta V(z)}$. The total bubble potential is $V(z) = V_i(z) + eFz$, F being the applied electric field and V_i the bubble potential energy due to the presence of the surface. In the ideal case of a sharp liquid-vacuum interface and neglecting both the bubble and the surface deformations when the bubble approaches the surface, one has $V_i = Qe^2/\epsilon z$. In Refs. 12 and 13 this ideal image potential form for V_i was assumed up to the surface.

This approach suffers from at least two main oversimplifications. First, as our results show, the electron potential $V_i(z)$ deviates greatly from the ideal image potential as the electron bubble comes sufficiently close to the surface layers, thus modifying the bubble distribution function where the tunneling rate is appreciable.

Moreover, we expect that $n \simeq n_{eq}$ only deep inside the liquid, where the bubble lifetime $[\tau_t(z) = p(z)^{-1}]$ is much larger than the collision time and therefore a Maxwell-Boltzmann distribution is a good approximation to the actual stationary distribution function. However, this may not be the case close to the surface where $p(z)$ can be quite large and the resulting distribution function may be different from the equilibrium one. In order to include both these effects, we must solve the full equation for the diffusion of bubbles under the actual potential $V_i(z)$ and with the tunneling process effective.

The distribution function $n(z,t)$ of the electron bubbles in the total potential $V(z) = V_i(z) + eFz$ is determined by the diffusion equation

$$\frac{\partial n(z,t)}{\partial t} + \frac{\partial J_z(z,t)}{\partial z} = -p(z)n(z,t), \tag{9}$$

where

$$J_z(z,t) = -\mu n(z,t)\frac{dV(z)}{dz} - D\frac{\partial n(z,t)}{\partial z} \tag{10}$$

is the bubble current density in the direction perpendicular to the surface. The loss term $-p(z)n(z,t)$ accounts for the bubbles disappearing due to electron tunneling from the liquid to the vapor. μ and D are the bubble mobility and diffusion coefficient, respectively, and they are related by Einstein's relation $\mu = \beta D$ ($\beta = 1/k_B T$). The experimental dependence of the mobility upon the temperature is given by $\mu = 8.62 \times 10^{-4} e^{8.45/T}$ cm^2/Vs, where T is the He temperature.[33]

To take into account the diffuseness of the liquid-vacuum interface and the full bubble structure, the ideal image potential V_i in V must be replaced by the total (i.e., electron + helium) potential energy variation as the electron bubble approaches the surface. Our calculated values for V_i are shown with dots in Fig. 6(a). For the purpose of integrating Eq. (9), we have fitted these points with a continuous curve, shown in Fig. 10, which has the correct asymptotic behavior at large z. Note that close to the surface the potential energy deviates dramatically from its ideal value. These variations, as we will show in the following, greatly affect the magnitude of the calculated decay rates of the electron current. The curve shown goes to zero at $z \sim R$, i.e., when the bubble "touches" the surface. The details of the curve close to this point are, however, quite irrelevant since only stable bubble positions will be considered in the following, i.e.,

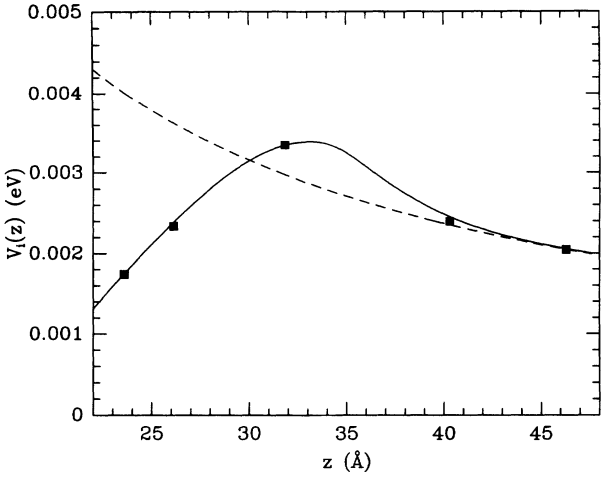

FIG. 10. Bubble potential energy curve. The squares show the calculated values, the solid line is a numerical fit to these points. The dashed line shows the ideal image potential $V_i = Qe^2/\epsilon z$.

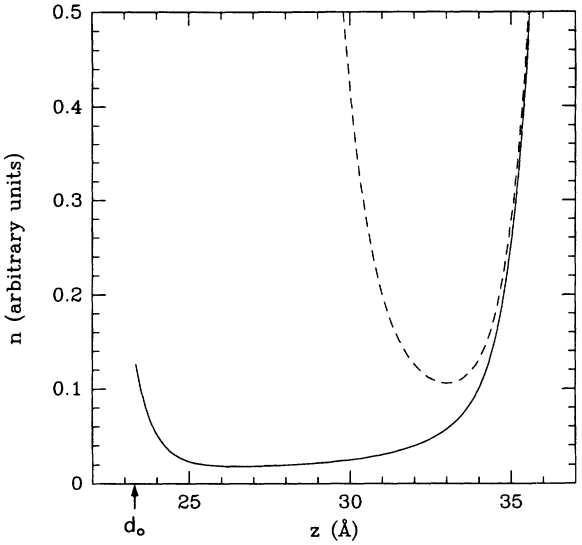

FIG. 11. Normalized bubble density distribution $n(z)$ corresponding to the potential of Fig. 10. Dashed line: $n_{eq} = Ae^{-\beta V}$; full line: n_0, stationary distribution, solution of Eq. (9) with boundary conditions as explained in text.

$z > d_0$, $d_0 \sim 23$ Å being the distance of closest approach corresponding to the leftmost point in Fig. 10.

Let us now consider a stationary solution of Eq. (9), $n_0(z)$. If we define $y(z) \equiv e^{\beta V/2} n_0(z)$, then $J_z = -De^{-\beta V/2}(\beta V' y/2 + y')$ (primes indicate derivatives with respect to z) and Eq. (9) becomes

$$-D[y'' + (\beta V''/2 - \beta^2 V'^2/4)y] = -p(z)y(z). \quad (11)$$

We solve the above equation with the boundary conditions $J_z(d_0) = 0$ and $J_z(L) = -J_\infty$, with J_∞ a positive constant. L is an arbitrary point located sufficiently far from the surface, where $p(z) = 0$. $J_z(L)$ is negative, corresponding to a flow of bubbles from inside the liquid towards the surface. This should represent the initial (stationary) state where the bubbles are injected into the bulk liquid by the electron source.

C. Current decay rates

Having obtained this particular solution, on the basis of the experimental observations[12] we assume that when the electron source in the liquid is switched off the total number of bubbles, $N(t) \equiv \int n(z,t)dz$, decays exponentially, i.e., $dN(t)/dt = -N(t)/\tau$. The decay rate $P = \tau^{-1}$ is then immediately obtained by integrating over z both sides of Eq. (9) with $J_z(L) = 0$ and $J_z(d_0) = 0$:

$$P = \frac{\int_{d_0}^{L} p(z) n_0(z) dz}{\int_{d_0}^{L} n_0(z) dz}. \quad (12)$$

The lifetimes $\tau = P^{-1}$ calculated according to Eq. (12) are much smaller than those provided by the theory of Refs. 12 and 13, but still from five to ten times larger than in the experiments, depending on the strength of the applied electric field.

We wish to stress the difference between our Eq. (12) and Eq. (8) used in Refs. 12 and 13. In our case the stationary, n_0, and not the equilibrium solution, $n_{eq} = Ae^{-\beta V}$, appears in the evaluation of the electron current decay rate. The two distributions are almost indistinguishable in the region near the surface if one uses the ideal image potential $V_i = Qe^2/\epsilon z$ as in Refs. 12 and 13, but, as shown in Fig. 11, they are quite different when they are determined by the more realistic potential of Fig. 10. In this last case, on approaching the surface the potential decreases sharply when $z \leq 33$ Å and correspondingly n_{eq} increases exponentially. In the same region, however, the tunneling process, whose rate also increases exponentially on approaching the surface, becomes very effective in destroying bubbles, and their stationary distribution n_0 is thus much smaller than the equilibrium one.

VI. CONCLUSIONS

We have studied the properties of an electron bubble close to the surface of liquid ^{4}He, by using a density-functional approach. We find that up to an electron-surface distance $d_0 \sim 23$ Å the bubble is stable, while at lower distances it becomes unstable and bursts. A potential energy barrier $\Phi/k_B \sim 38$ K for the thermal emission of electrons is obtained from our results, in agreement with experiments. Even when the electron-surface distance is larger than d_0, however, tunneling through the surface layer dominates the electron escape probability. Large deviations of the electron potential energy from its ideal value are found close to the surface. These deviations have a profound effect on the calculated current decay lifetimes, which are much smaller than those

obtained previously and in semiquantitative agreement with experiments.

We see two possible reasons for the remaining discrepancy between theory and experiment. Our use of a continuum model for describing the liquid, even when the bubble is only two He layers from the surface, is an approximation which could affect both our estimate of the tunneling rates and of the electron-bubble energy in the very region where these two quantities are crucial for the evaluation of the current decay rate.

A second question to be investigated deals with the assumption at the basis of Eq. (12), namely of a single decay time for the current. As a matter of fact, Eq. (12) describes only the initial decay rate, just after the injection of electrons is switched off. One should investigate whether this is the dominant decay time or whether other decay times determine the experimental measurement.

Both these problems are currently under study.

ACKNOWLEDGMENTS

One of the authors (F.A.) wishes to thank F. A. Borghesani for a useful discussion. This work has been supported by the Italian Ministero della Pubblica Istruzione through the Consorzio Nazionale di Fisica della Materia and the Consiglio Nazionale delle Ricerche through Progetto Finalizzato "Sistemi Informatici e Calcolo Parallelo."

[1] For a comprehensive review of electron states in helium, see for instance, M.W. Cole, Rev. Mod. Phys. **46**, 451 (1974); A.L. Fetter in *The Physics of Liquid and Solid Helium*, edited by K.H. Bennemann and J.B. Ketterson (Wiley, New York, 1974); K.W. Schwarz, in *Advances in Chemical Physics* XXXIII, edited by L. Prigogine and S. A. Rice (Wiley, New York, 1975); J.P. Hernandez, Rev. Mod. Phys. **63**, 675 (1991).

[2] R.A. Ferrel, Phys. Rev. **108**, 167 (1957).

[3] C.C.Grimes and G. Adams, Phys. Rev. B **45**, 2305 (1992).

[4] M.A. Woolf and G.W. Rayfield, Phys. Rev. Lett. **15**, 235 (1965).

[5] J. Poitrenaud and F.I.B. Williams, Phys. Rev. Lett. **29**, 1230 (1972); **32**, 1213(E) (1974).

[6] Y.M. Shih and C.W. Woo, Phys. Rev. Lett. **8**, 1437 (1973).

[7] T.C. Padmore and M.W. Cole, Phys. Rev. A **9**, 802 (1974).

[8] L. Bruschi, B. Maraviglia, and F.E. Moss, Phys. Rev. Lett. **17**, 682 (1966).

[9] W. Schoepe and C. Probst, Phys. Lett. **31A**, 490 (1970).

[10] H.M. Huang, Y.M. Shih, and C.W. Woo, J. Low. Temp. Phys. **14**, 413 (1974).

[11] G.W. Rayfield and W. Schoepe, Phys. Lett. **34**A, 133 (1971); Z. Naturforsch. Teil A **26**, 1392 (1971).

[12] W. Schoepe and G.W. Rayfield, Phys. Rev. A **7**, 2111 (1973).

[13] M.W. Cole and J.R. Klein, J. Low Temp. Phys. **36**, 331 (1979).

[14] J. Bardeen, Phys. Rev. Lett. **6**, 57 (1961).

[15] S. Stringari and J. Treiner, Phys. Rev. B **36**, 8369 (1987).

[16] L.B. Lurie, T.A. Rabedeau, P.S. Pershan, I.F. Silvera, M. Deutsch, S.D. Kosowsky, and B.M. Ocko, Phys. Rev. Lett. **68**, 2628 (1992); **72**, 309(E) (1992).

[17] V.R. Pandharipande, S.C. Pieper, and R.B. Wiringa, Phys. Rev. B **34**, 4571 (1986).

[18] J. Dupont-Roc, M. Himbert, N. Pavloff, and J. Treiner, J. Low. Temp. Phys. **81**, 31 (1990).

[19] B.N. Miller and T. Reese, Phys. Rev. A **39**, 4735 (1989).

[20] N.R. Kestner, J. Jortner, M.H. Cohen, and S.A. Rice, Phys. Rev. **140**, A56 (1965).

[21] For a review, see, e.g., G. Galli and A. Pasquarello, *New Perspectives on Computer Simulations in Chemical Physics* (Kluwer, Dordrecht, 1994).

[22] F. Ancilotto, A. Selloni, and R. Car, Phys. Rev. Lett. **71**, 3685 (1993).

[23] I. Stich, R. Car, M. Parrinello and S. Baroni, Phys. Rev. B **39**, 4997 (1989).

[24] T. Miyakawa and D.L. Dexter, Phys. Rev. A **1**, 513 (1970).

[25] W.T. Sommer, Phys. Rev. Lett. **12**, 271 (1964).

[26] J.R. Broomall, W.D. Johnson, and D.G. Onn, Phys. Rev. B **14**, 2819 (1976).

[27] B. Space, D.F. Coker, Z.H. Liu, B.J. Berne, and G. Martyna, J. Chem. Phys. **97**, 2002 (1992).

[28] C. Ebner and W.F. Saam, Phys. Rev. B **12**, 923 (1975).

[29] A time-dependent, fully self-consistent calculation of the escape process would be prohibitively costly.

[30] M. Buttiker and R. Landauer, Phys. Rev. Lett. **49**, 1739 (1982).

[31] Even in the case of closest approach of the electron bubble to the surface [see panel (c) in Fig. 5] the potential energy barrier which keeps the electron inside the bubble cavity is sufficiently high with respect to the electron energy E_e to ensure the applicability of the transfer Hamiltonian theory, which is valid for thick and/or high potential barriers.

[32] We have determined the ground-state energy for an electron bound by this potential and found $E_0 = -0.64$ meV, i.e., very close to the one-dimensional hydrogenic value $E_0^{\mathrm{H}} = -Q^2e^2/2a_0 = -0.67$ meV expected in the case of an abrupt, infinitely repulsive, planar surface Ref. 1. The wave function is also almost coincident with the hydrogenlike s wave function, $\Psi_0^{\mathrm{H}} = 2a^{-3/2}ze^{-z/a}$, apart from a very small penetration tail into the liquid.

[33] L. Bruschi (private communication).